Depth Profiling of Charging Effect of Si Nanocrystals Embedded in SiO2: A Study of Charge Diffusion among Si Nanocrystals

Y. Liu,[†] T. P. Chen,*[,†] C. Y. Ng,[†] L. Ding,[†] S. Zhang,[‡] Y. Q. Fu,[‡] and S. Fung[§]

School of Electrical and Electronic Engineering, Nanyang Technological University, Singapore 639798, Singapore, School of Mechanical and Aerospace Engineering, Nanyang Technological University, Singapore 639798, Singapore, and Department of Physics, The University of Hong Kong, Hong Kong

Received: May 10, 2006; In Final Form: June 29, 2006

Si nanocrystal (nc-Si) embedded in SiO2 thin film is synthesized with low-energy Si ion implantation. Depth profiling of the charging effect of the nc-Si is determined from X-ray photoemission measurement. It is observed that there is a strong correlation between the depth profile of the charging effect and the nc-Si depth distribution. The charging effect is found to decrease with the increase of nc-Si concentration and to vanish when a densely stacked nanocrystal layer is formed. The phenomenon is attributed to the charge diffusion among the nanocrystals. The charge diffusion in the nanocrystal layer may have an important implication for nanocrystal flash memory. When such a layer is used as the charge-storage layer in the memory cells, the stored charges could be lost due to the rapid charge diffusion among the nc-Si if a single defect exists in the tunneling oxide, causing a reliability problem in data retention.

Si nanocrystals (nc-Si) embedded in a SiO_2 thin film have been studied extensively due to their applications in nonvolatile memory devices.[1−8] Ion implantation is a promising technique for synthesizing the structure of nc-Si in SiO2 films because of its ability to control the nanocrystal distribution and its full compatibility with the mainstream complementary metal-oxide-semiconductor (CMOS) process. For the application of nonvolatile memory devices, a high-dose low-energy Si ion implantation into a thin SiO2 film allows for the formation of the charge storage layer located within the direct tunneling distance from the SiO2/Si substrate interface. As the charge storage layer is a layer of discrete and mutually isolated nc-Si embedded in the gate oxide, it is believed that a single defect in the tunnel oxide will not cause charge lose of the entire nc-Si layer in the device. However, based on the depth profile of the charging effect in the nc-Si determined from the X-ray photoelectron spectroscopy (XPS) measurement in the present study, the charging effect is found to vanish in the region with a high nc-Si concentration. This situation is due to the formation of a densely stacked nc-Si layer[8] in the region. In such a nc-Si layer charges can diffuse from the charged nc-Si to neighboring uncharged nc-Si easily and thus localized charging is reduced. This suggests that the charges stored in the entire nc-Si layer in the memory cell could be lost due to the charge diffusion among the nc-Si if a single defect exists in the underlying tunneling oxide.

A 30 nm SiO2 thin film was thermally grown in dry oxygen at 950 °C on a p-type Si(100) wafer. Si^+ ions with a dose of 8×10^{16} cm^{-2} were then implanted into the SiO2 thin film at 1 keV. Thermal annealing was carried out in N_2 ambient at 1000 °C for 80 min to induce nc-Si formation. XPS measurement was performed by using a Kratos AXIS spectrometer with monochromatic Al Kα (1486.71 eV) X-ray radiation. Si 2p core level spectra were recorded at various depths. C 1s spectra due to the surface carbon contamination were also rerecorded as a reference for the X-ray-induced charging effect on the sample surfaces. The depth profiling was achieved by Ar ion sputtering, which was carried out with the XPS measurement in situ. The XPS data were recorded every 1 nm in depth.

The depth distribution of the implanted Si in the SiO2 thin film after the annealing has been determined with both the secondary ion mass spectroscopy (SIMS) and the stopping and range of ions in matter (SRIM) simulation, and the results are also compared with the sum of the relative concentrations of Si nanocrystal (Si^0) and the Si suboxides (Si^{n+}, $n = 1$, 2, and 3) determined from the XPS analysis, as shown in Figure 1a. As can be seen in the figure, the results obtained with the three different techniques are consistent, and the excess Si is mainly distributed from the depth of ∼2 nm to the depth of ∼10 nm with the peak concentration located at the depth of 4−6 nm. Note that there is not much change in the depth profile after a thermal annealing due to the very low Si diffusion rate in the SiO2 matrix.[9] On the other hand, a densely stacked nc-Si layer (i.e., the above-mentioned region of the depths of ∼2 to ∼10 nm) can be clearly seen in the transmission electron microscopy (TEM) image that is shown in Figure 1b.

It has been known that X-ray irradiation can cause charging in both the SiO2/Si system[10−12] and the nc-Si/SiO2 system.[13−15] For the system of nc-Si embedded in a SiO2 matrix, photoemission will leave positive charges in the nanocrystals, leading to a core-level shift to a higher binding energy. The C 1s core level shift shown in Figure 2 is an indicator of the charging effect. The C 1s core level on pure SiO2 surface has a shift of ∼0.8 eV relative to the C 1s reference, while it shows a shift of ∼1.9 eV on the surface of the sample of nc-Si embedded in SiO2. This indicates that the charging effect is greatly enhanced by the introduction of nc-Si into the SiO2 matrix. To monitor the charging effect underneath the surface, C 1s cannot be used as there is no sufficient carbon impurity below a certain depth

* Address orrespondence to this author. E-mail: echentp@ntu.edu.sg.
[†] School of Electrical and Electronic Engineering, Nanyang Technological University.
[‡] School of Mechanical and Aerospace Engineering, Nanyang Technological University.
[§] Department of Physics, The University of Hong Kong.

10.1021/jp062852c CCC: $33.50
Published on Web 08/02/2006

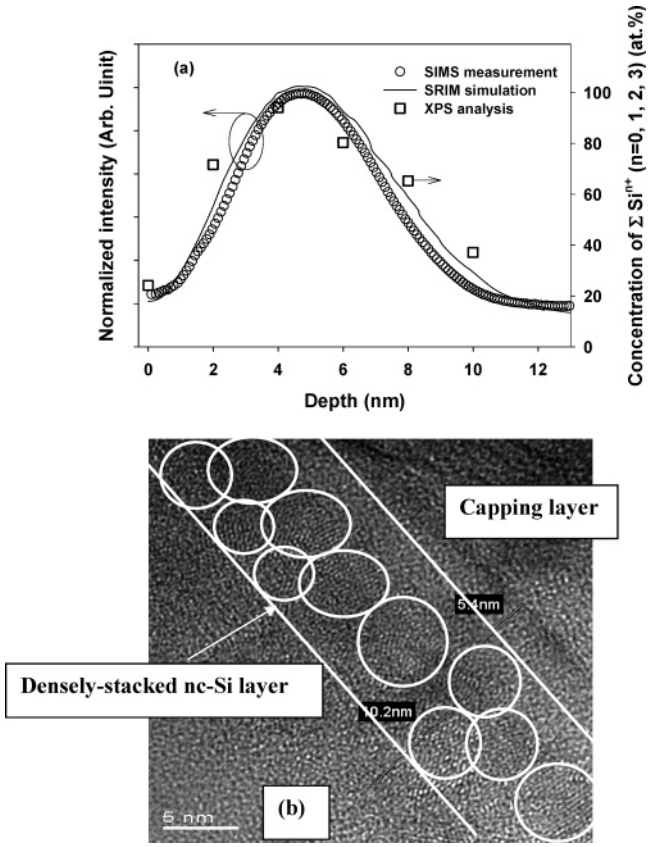

Figure 1. (a) Depth profile of implanted Si in the SiO2 thin film obtained from the SRIM simulation and SIMS measurement. The sum of the relative concentrations of Si nanocrysal (Si^0) and the Si suboxides (Si^{n+}, $n = 1$, 2, and 3) determined from the XPS analysis is also included for comparison. (b) TEM image of the nanocrystals embedded in the SiO2 thin film.

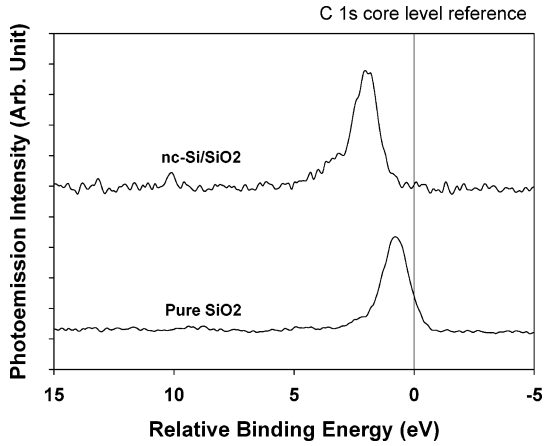

Figure 2. C 1s spectra obtained from the surfaces of the samples with and without nc-Si.

in the Si-implanted SiO2 sample. However, as discussed later, the core level shift of the oxidation state of Si^{4+}, which is caused by the charging effect, can be used for the depth profiling of the charging effect.

Panels a−c in Figure 3 show the XPS Si 2p core level peaks obtained on the surface and at the depths of 4 and 8 nm, respectively. Five oxidation states Si^{n+} ($n = 0$, 1, 2, 3, and 4) corresponding to the five chemical structures including Si (i.e., Si nanocrystal here), Si_2O, SiO, Si_2O_3, and SiO_2, respectively, could exist in the Si-implanted SiO2 films.[13,14] With the possible

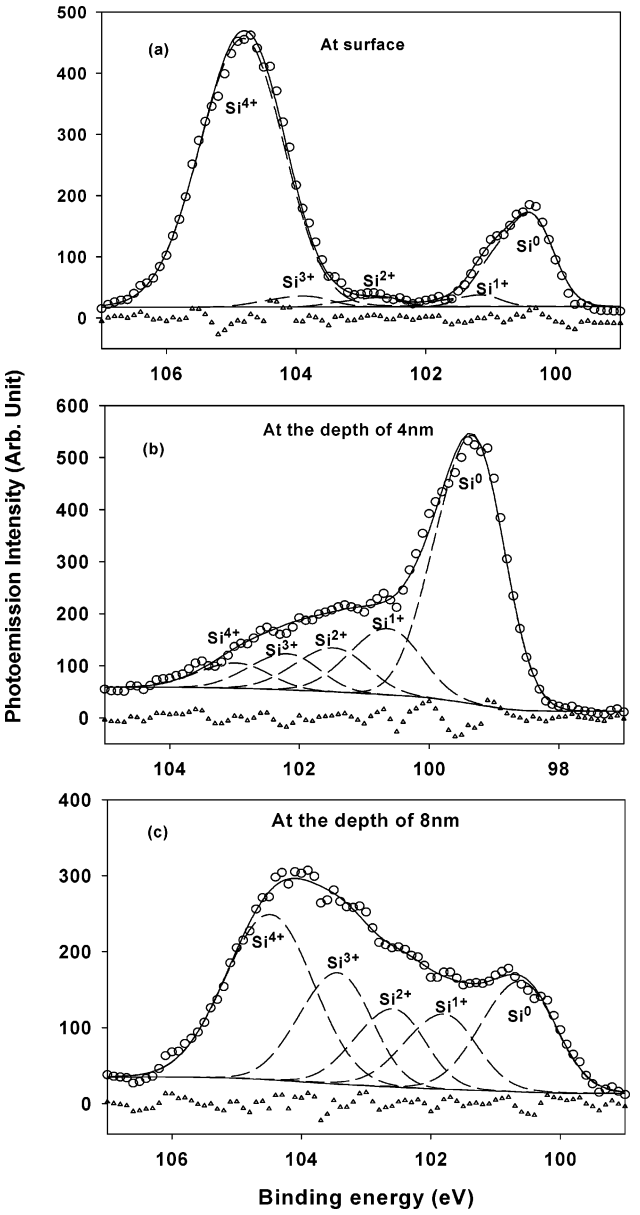

Figure 3. Deconvolution of Si 2p spectra obtained on the surface (a), at the depth of 4 nm (b), and at the depth of 8 nm (c). The unfilled triangles represent the difference between the curve fitting and the measurement.

existence of the five oxidation states in mind, we have carried out the curve fitting by decomposing the spectrum into the Si $2p_{1/2}$ and $2p_{3/2}$ partner lines for the five oxidization states following the reported fitting procedure.[16−18] The spin−orbit splitting is fixed at 0.6 eV and the Si $2p_{1/2}$ and $2p_{3/2}$ intensity ratio is set to $^1/_2$ for all of the five oxidation states.[19] For a clear presentation, the Si $2p_{1/2}$ and $2p_{3/2}$ partner lines are recombined into one peak for all five oxidation states in Figure 3. The XPS Si 2p spectra at different depths are deconvoluted based on the above approach. The deconvolution of the spectra on the surface and at the depths of 4 and 8 nm is also shown in Figure 3.

As can be observed in Figure 3, the peak areas of the five oxidation states change with the depth, showing that the concentrations of the five oxidation states vary with the depth. The depth profile of the relative concentration of each oxidation state can be obtained by calculating the ratio of (I_{Si}^{n+}/I_{total}) ($n = 0$, 1, 2, 3, and 4) at various depths where I_{Si}^{n+} is the peak

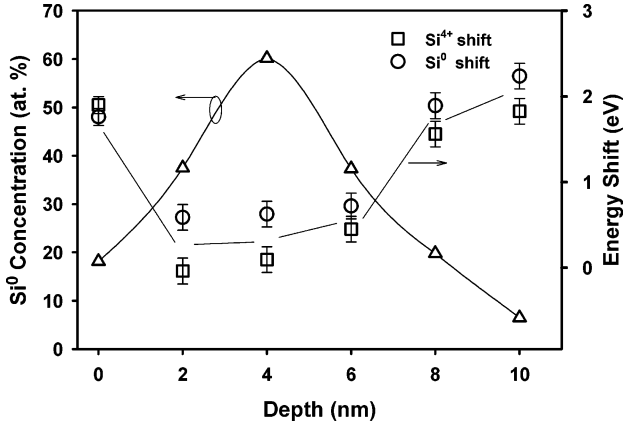

Figure 4. Si^{4+} and Si^0 shifts relative to the references (i.e., the Si 2p core level in pure SiO2 and the Si 2p core level in bulk Si) at various depths. The depth profile of nc-Si (i.e., the Si^0) concentration is included for comparison. The triangles, squares and circles represent the nc-Si concentration, the Si^{4+} shift, and the Si^0 shift, respectively.

area of the oxidation state Si^{n+} and I_{total} is the total area ($=\sum_{i=0}^{4} I_{Si^{n+}}$) of the Si 2p peaks. The sum of the relative concentrations of the Si nanocrystal (Si^0) and the Si suboxides (Si^{n+}, n=1, 2 and 3) versus the depth is also shown in Figure 1a. As can be observed from the figure, it is consistent with the SRIM simulation and the SIMS measurement.

Besides the concentrations of the five oxidation states, the binding energy of each oxidation state also can be obtained from the peak deconvolution mentioned above. The core-level shift of Si^{4+} relative to the reference (i.e., Si 2p in pure SiO2 [10]) as a function of the depth is shown in Figure 4. A shift of ~1.9 eV on the surface is observed. This shift coincides with the C 1s shift (~1.9 eV) on the sample surface. As discussed early, the C 1s shift is due to the charging effect induced by the photoemission. On the other hand, Si^{4+} represents the host material (i.e., SiO2) in the material system under study. Obviously, the charging effect in the material system will cause a shift in the Si^{4+} binding energy. Therefore, the Si^{4+} shift is used for monitoring the charging effect, and the variation of the Si^{4+} shift with the depth, which is shown in Figure 4, actually represents the depth profile of the charging effect. On the other hand, the Si^0 (representing the Si nanocrystal) shift could be due to both the charging effect and the quantum confinement effect of the Si nanocrystal, as discussed later.

To understand the depth profile of the charging effect, the depth distribution of the concentration of Si^0 (i.e., the Si nanocrystal), which is determined from the peak deconvolution, is also shown in Figure 4 for comparison. As can be seen in the figure, most of the nanocrystals are confined in the region of the depths of ~2 to ~6 nm. A strong correlation of the charging effect with the Si^0 concentration is observed from the figure. From the surface to the depth of ~2 nm, with the increase of the nanocrystal concentration, the Si^{4+} shift decreases from ~1.9 eV on the surface to almost zero at the depth of ~2 nm; in the region of the nanocrystal layer (i.e., the depths of ~2 to ~6 nm), the shift is zero or very small; and in the region deeper than ~6 nm, the shift increases again with the reduction in the nanocrystal concentration. This suggests that the charging effect is reduced with the increase of nanocrystal concentration and can vanish when a densely stacked nanocrystal layer is formed. The Si^0 shift relative to the reference of bulk crystalline Si as a function of the depth is also shown in Figure 4. The Si^0 shift follows the trend of the Si^{4+} shift, but it is slightly larger than the shift of Si^{4+}. As both the photoemission-induced charging

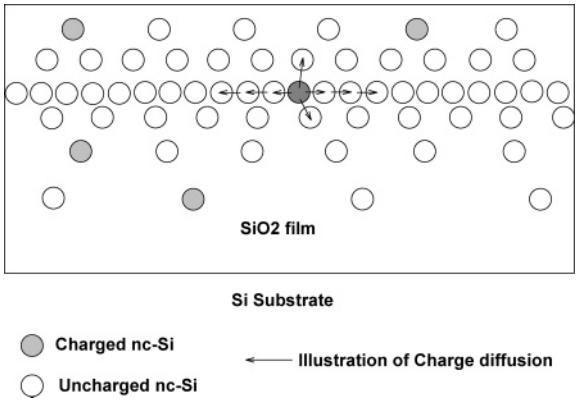

Figure 5. Illustration of charge diffusion from the charged nc-Si to the adjacent uncharged nc-Si.

in the nc-Si and the quantum size effect on the Si^0 core level[20,21] could shift the core level to a higher binding energy, the Si^0 shift would be larger than the shift of Si^{4+}.

The influence of the nanocrystal distribution on the charging effect is explained in the following. As illustrated in Figure 5, charge diffusion can take place due to the charge transfer from the charged nanocrystals to the adjacent uncharged nanocrystals by tunneling or other transport mechanisms. In the densely stacked nanocrystal layer, the charge induced by the photoemission can easily diffuse out to the nanocrystals that are not under the X-ray illumination, and thus the charge can be dissipated quickly, leading to a drastic reduction in the charging effect. For those nanocrystals distributed in the surface region and in the region deeper than ~10 nm, their concentrations are much lower, they are separated from each other with a larger spacing, and thus the charge diffusion is much more difficult to occur. Therefore, the charging effect is much more significant in the two regions.

The rapid charge diffusion in the densely stacked nanocrystal layer may have an important implication for nanocrystal flash memory devices in which the nanocrystal layer is synthesized with ion implantation. In such a device, to achieve a large memory window, a high-dose (normally more than 2×10^{16} cm^{-2}) low-energy (lower than ~2 keV) ion implantation into a SiO2 thin film is used to synthesize the nanocrystal layer embedded in the gate oxide.[7,8,22,23] It is generally believed that the stored charge is maintained in the individual nanocrystal such that a single defect in the tunnel oxide will not cause the charge lose of the entire nanocrystal layer within the device. However, with the rapid charge diffusion in the nanocrystal layer, the entire nanocrystal layer could be discharged via the defect leakage path, leading to a serious problem in charge retention.

In conclusion, for nc-Si embedded in a SiO2 thin film synthesized with low-energy ion implantation, there is a strong correlation between the depth profile of the charging effect and the nc-Si depth distribution. The charging effect is reduced with the increase of nc-Si concentration, and it is found to vanish when a densely stacked nanocrystal layer is formed. The phenomenon is attributed to the charge diffusion due to the charge transfer from the charged nanocrystals to the adjacent uncharged nanocrystals. In the densely stacked nanocrystal layer, the charge induced by the photoemission can easily diffuse out to the nanocrystals that are not under the X-ray illumination, and thus the charge can be dissipated quickly, leading to a drastic reduction in the charging effect. This may have an important implication for nanocrystal flash memory. When such a layer

is used as the charge-storage layer in a memory cell, the stored charge could be lost due to the rapid charge diffusion among the nc-Si if a defect exists in the underlying tunneling oxide, causing a reliability problem in data retention.

Acknowledgment. This work has been financially supported by the Ministry of Education, Singapore, under project ARC 1/04 and by the Singapore Millennium Fund.

References and Notes

(1) Lu, T. Z.; Alexe, M.; Scholz, R.; Talelaev, V.; Zacharias, M. *Appl. Phys. Lett*. **2005**, *87*, 202110.

(2) González-Varona, O.; Garrido, B.; Cheylan, S.; Pérez-Rodríguez, A.; Cuadras, A.; Morante, J. R. *Appl. Phys. Lett*. **2003**, *82*, 2151.

(3) Brault, J.; Saitoh, M.; Hiramoto, T. *IEEE Trans. Nanotechnol*. **2005**, *4*, 349.

(4) Normand, P.; Kapetanakis, E.; Dimitrakis, P.; Skarlatos, D.; Tsoukalas, D.; Beltsios, K.; Claverie, A.; Benassayag, G.; Bonafos, C.; Carrada, M.; Cherkashin, N.; Soncini, V.; Agarwal, A.; Sohl, Ch.; Ameen, M. *Microelectron. Eng.* **2003**, *67*−*68*, 629.

(5) Gebel, T.; Borany, J. von; Thees, H.-J.; Wittmaack, M.; Stegemann, K.-H.; Skorupa, W. *Microelectron. Eng.* **2001**, *59*, 247.

(6) Liu, Y.; Chen, T. P.; Ng, C. Y.; Ding, L.; Tse, M. S.; Fung, S.; Tseng, A. A. *IEEE Trans.* Electron. Devices **2006**, *53*, 914.

(7) Ng, C. Y.; Chen, T. P.; Yang, M.; Yang, J. B.; Ding, L.; Li, C. M.; Du, A.; Trigg, A. *IEEE Trans. Electron. Devices* **2006**, *53*, 663.

(8) Ng, C. Y.; Chen, T. P.; Ding, L.; Fung, S. *IEEE Electron. Device Lett.* **2006**, *27*, 231.

(9) López, M.; Garrido, B.; Bonafos, C.; Pérez-Rodríguez, A.; Morante, J. R. *Solid-State Electron*. **2001**, *45*, 1495.

(10) Iwata, S.; Ishizaka, A. *J. Appl. Phys*. **1996**, *79*, 6653.

(11) Ulgut, B.; Suzer, S. *J. Phys. Chem. B* **2003**, *107*, 2939.

(12) Karadas, F.; Ertas, G.; Suzer, S. *J. Phys. Chem. B* **2003**, *108*, 1515.

(13) Liu, Y.; Chen, T. P.; Fu, Y. Q.; Tse, M. S.; Hsieh, J. H.; Ho, P. F.; Liu, Y. C. *J. Phys. D*: *Appl. Phys.* **2003**, *36*, L97.

(14) Chen, T. P.; Liu, Y.; Sun, C. Q.; Tse, M. S.; Hsieh, J. H.; Fu, Y. Q.; Liu, Y. C.; Fung, S. *J. Phys. Chem. B* **2004**, *108*, 16609.

(15) Dane, A.; Demirok, U. K.; Aydinli, A.; Suzer, S. *J. Phys. Chem. B* **2006**, *110***,** 1137**.**

(16) Crist, V. *J. Surf. Anal*. **1999**, *4*, 428.

(17) Hesse, R.; Chasse, T.; Szargan, R. *Fresenius' J. Anal. Chem*. **1999**, *365*, 48.

(18) Tay, Y. Y.; Li, S.; Sun, C. Q.; Chen, P. *Appl. Phys. Lett.* **2006**, *88*, 173118.

(19) Himpsel, F. J.; McFeely, F. R.; Taleb-Ibrahimi, A.; Yarmoff, J. A.; Hollinger, G. *Phys. Rev. B* **1988**, *38*, 6084.

(20) Ögüt, S.; Chelikowsky, J. R.; Louie, S. G. *Phys. Rev. Lett.* **1997**, *79*, 1770.

(21) Sun, C. Q.; Tay, B. K.; Fu, Y. Q.; Li, S.; Chen, T. P.; Bai, H. L.; Jiang, E. Y. *J. Phys. Chem. B* **2003**, *107*, 411.

(22) Kapetanakis, E.; Normand, P.; Tsoukalas, D.; Beltsios, K.; Stoemenos, J.; Zhang, S.; Berg, J van den *Appl. Phys. Lett.* **2000**, *77*, 3450.

(23) Normand, P.; Kapetanakis, E.; Dimitrakis, P.; Tsoukalas, D.; Beltsios, K.; Cherkashin, N.; Bonafos, C.; Benassayag, G.; Coffin, H.; Claverie, A.; Soncini, V.; Agarwal, A.; Ameen, M. *Appl. Phys. Lett.* **2003**, *83*, 168.